Materials Science and Engineering C 35 (2014) 61–69

Contents lists available at ScienceDirect

Materials Science and Engineering C

journal homepage: www.elsevier.com/locate/msec

Antimicrobial hyperbranched poly(ester amide)/polyaniline nanofiber modified montmorillonite nanocomposites

Sujata Pramanik [a], Pranjal Bharali [b], B.K. Konwar [b], Niranjan Karak [a,*]

[a] Advanced Polymer and Nanomaterial Laboratory, Department of Chemical Sciences, Tezpur University, Tezpur 784028, India
[b] Department of Molecular Biology and Biotechnology, Tezpur University, Tezpur 784028, India

ARTICLE INFO

Article history:
Received 22 August 2013
Received in revised form 19 September 2013
Accepted 19 October 2013
Available online 31 October 2013

Keywords:
Polyaniline nanofiber
Montmorillonite
Nanocomposite
Mechanical properties
Antimicrobial activity

ABSTRACT

There has been growing interest in the use of nanomaterials featuring potent of antimicrobial activity in the biomedical domain. It still remains a challenge for the researchers to develop an efficient nanocomposite possessing antimicrobial efficacy against broad spectrum microbes including bacteria, fungi as well as algal consortium, posing serious challenges for the human survival. In addressing the above problem, we report the fabrication of bio-based hyperbranched poly(ester amide) (HBPEA)/polyaniline nanofiber modified montmorillonite (MMT) nanocomposites by an ex-situ polymerization technique at varied weight percentages (1, 2.5, 5 wt.%) of the modified MMT (nanohybrid). The Fourier transform infrared spectroscopy confirmed the structural changes upon interaction of the nanohybrid with HBPEA. A probable mechanism is proposed for the formation of nanocomposites with partially exfoliated nanoplatelet structure, which was further confirmed from the high resolution transmission electron microscopic analyses. The prepared nanocomposites exhibited potent efficacy against gram positive bacteria like *Bacillus subtilis* and *Staphylococcus aureus* as compared to the gram negative ones like *Pseudomonas aeruginosa* and *Escherichia coli*. The nanocomposites showed significant antifungal activity against *Aspergillus niger*, *Fusarium oxysporum* and *Coleotricum capcii* and antialgal activity against algal consortium comprising of *Chlorella*, *Hormidium* and *Cladophorella* species. The formation of thermosetting nanocomposites resulted in the acceptable improvement of desired physico-chemical and mechanical properties including thermostability. Thus pronounced antimicrobial activity of the nanocomposites against a spectrum of bacterial and fungal strains as well as a consortium of algal species along with other desired performance vouched them as potent antimicrobial materials in the realm of health and biomedical industry.

1. Introduction

Mankind has been constantly interacting with the world of microorganisms — one of the most deadly 'enemies' confronted by the human. The adherence of the microorganisms to the surfaces poses infection and device failure problems in the biomedical equipments, and many other domains such as healthcare products, food packaging, textile industry and so on [1,2]. Thus modification of surfaces to impart antimicrobial property for inhibiting the growth of detrimental microbial pathogens is the need of hour. The antimicrobial coating technology offers cutting-edge solutions for applications in the realm of health and biomedical industry, food processing industry and so on [2]. The 'oligodynamic effect' (which states that antimicrobial efficacy) of metal ions like mercury, silver, copper, iron, lead, zinc, bismuth, gold, and aluminum is known for centuries and it is based on the interaction of the released metal ions with specific microbial species [3]. The epidemic of microbial resistance in the microorganisms has seriously complicated the existence of the conventional antimicrobial materials and caused the necessity to explore new and effective antimicrobial materials [4]. The quest for the cost-effective and efficient materials possessing potent antimicrobial efficacy against a wide spectrum of microorganisms has fetched considerable interest in the various industrial and biomedical domains. In this context, the antimicrobial potency of π-conjugated polymers, particularly polyaniline (PAni) has been widely reported in literature [5]. A promising route to control and enhance the properties of PAni is to organize these polymeric chains in the nanoscale regime [6]. Moreover the nanostructured PAni has received great impetus in the recent years because of the increment of the interaction of the same with the target organism as compared to their bulk analogs [7].

Recently research interest has been focused on the application of montmorillonite (MMT)-based antimicrobial materials due to the global concern on the use of such resources to avert the detrimental attributes of the microbial pathogens. Amidst the layered sorption materials, MMT is an economically viable and versatile to be effective in intercalating nanostructured antimicrobial material by either ion-exchange or covalent bonding mechanisms [8]. The silicate galleries of the MMT represent a preferred substrate for the anchoring and adsorption/absorption within their interlamellar spaces because of its high cation exchange capacity (CEC) with high surface area and swelling ability [9]. The use of

* Corresponding author. Tel.: +91 3712 267009; fax: +91 3712 267006.
E-mail address: karakniranjan@yahoo.com (N. Karak).

0928-4931/$ – see front matter
http://dx.doi.org/10.1016/j.msec.2013.10.021

organically modified antimicrobial MMT has greater advantages including low toxicity over the inorganic antimicrobial material modified MMT [10]. In this milieu, MMT is viewed to be a low cost, ecologically compatible and effective scaffold material for the intercalation of PAni nanofiber. PAni modified MMT system (nanohybrid) — a potent antimicrobial nanomaterial, thus, constitutes a group of multilayered nanomaterials in which PAni chains are sandwiched between nanoclay layers [11–13]. However the potential leaching of the antimicrobial agents results in decreased efficiency of the same for long term applications [14]. It still remains a challenge to the researchers to develop an efficient antimicrobial material possessing long term efficacy.

Against the perspective outlined above, an attempt to prepare antimicrobial materials by inclusion of the above nanohybrid into a bio-based hyperbranched poly(ester amide) resin (HBPEA) [15] is an interesting proposition. The HBPEA plays an influential role in the interaction with the nanohybrid due to the presence of multitude of functional groups, three dimensional unique structural architecture, high reactivity and high compatibilizing ability over their linear analogs. The hydrophobic organo-modified MMT is essential for the preparation of the HBPEA nanocomposites because the organic modifier facilitates the intercalation of hydrophobic polymer into the MMT layers by reducing the surface energy [16]. The fabrication of such nanocomposites results in antimicrobial activity along with desirable other attributes like mechanical and thermal which support to find uses in myriad of applications including coatings for biomedical application. Such polymer nanocomposites are classified as a combination of third and fourth category of 'polymeric materials with antimicrobial activity' incorporating organic–inorganic antimicrobial agents into the HBPEA matrix [17]. A perusal of literature has shown that the fabrication of nanocomposites of bio-based HBPEA and nanohybrid has not been strived for, which urged us to initiate the present study.

Thus in continuation of our exploration of the nanohybrid, herein we wish to report the fabrication of nanocomposites of HBPEA/nanohybrid at varied loadings of 1, 2.5 and 5 wt.% of the nanohybrid via ex-situ polymerization technique. FTIR, HRTEM and XRD tools were used to investigate the interaction of the nanohybrid with HBPEA. The mechanical properties and thermal stability of the nanocomposites were also delved into. Further the antimicrobial efficacy of the prepared nanocomposites was investigated against a spectrum of bacterial and fungal strains as well as an algal consortium in order to find out their suitability as antimicrobial materials.

2. Materials and methods

2.1. Materials

Aniline ($C_6H_5NH_2$) was purchased from Merck, India and purified by vacuum distillation in the presence of zinc dust (S.D. Fine-Chem Ltd, India) and kept at low temperature prior to use. Ammonium peroxydisulfate (APS) and hydrochloric acid (HCl) (11.6 N) were used as purchased (Merck, India). Hydrophilic MMT (Nanomer® PGV, Sigma-Aldrich) with cation exchange capacity (CEC) of 89 m equiv./100 g was used as received. Castor oil (Sigma Aldrich, India), diethanol amine (Merck, India), phthalic anhydride (Merck, India) and isophthalic acid (Sisco Research Laboratory Pvt. Ltd., India) were used after drying in vacuo at 50 °C for overnight. Maleic anhydride (Merck, Germany) was used after drying in a vacuum oven at 30 °C. The bisphenol-A-based epoxy resin (BPA, Araldite GY 250) (epoxy equivalent — 180–190 g/equiv. and density 1.16 g/cm^3 at 25 °C) and poly(amido amine) hardener (HY 840) were procured from Hindustan Ciba Geigy Ltd., Mumbai and used as received. N,N-dimethylacetamide (DMAc), dimethylformamide (DMF) and tetrahydrofuran (THF) were purchased from Merck, India and distilled before use. The bacterial and algal strains used in the present investigation were collected from the Department of Molecular Biology and Biotechnology, Tezpur University. The fungal strains were brought from the Department of Mycology, Assam Agricultural University, India.

2.2. Ex-situ preparation of nanocomposites of castor oil based HBPEA/nanohybrid

2.2.1. Preparation of nanohybrid

MMT was modified via organo-cation exchange reaction using PAni nanofiber. The nanohybrid was prepared by in-situ intercalative polymerization technique as reported earlier by the same authors [13], following absorption of anilinium salt onto the MMT layers and their subsequent polymerization using APS as the oxidant.

2.2.2. Preparation of nanocomposites of castor oil based HBPEA/nanohybrid

The methyl ester of the castor oil prepared by transesterification reaction was reacted with diethanol amine in the presence of sodium methoxide catalyst to obtain fatty amide of the oil [18]. The HBPEA was synthesized using $A_2 + B_2 + A'A_2$ approach, details of which have been described elsewhere [15]. Briefly, the fatty amide of the oil and the diacids/anhydrides like maleic anhydride, phthalic anhydride and isophthalic acid as A_2 as B_2 monomers, respectively, reacted with diethanol amine, the $A'A_2$ monomer. The mole ratio of the unsaturated and saturated diacids/anhydrides was maintained at 30:70 (keeping equal mole ratio of the saturated diacid/anhydrides). This $A'A_2$ and A_2 monomer reacts with the B_2 monomer to yield $A_2B/BA'A$ as the intermediate during the reaction, which helped avert the gelation. The resinification reaction was carried out at 150 °C for 30 min followed by heating at 185 °C for another 1.5 h and finally at 220–225 °C for 20–25 min with continuous mechanical stirring under the blanket of nitrogen. The reaction temperature was brought to 60–65 °C and then the nanohybrid dispersed in THF was added to the above resin in varying weight percentages of 1, 2.5 and 5 wt.% separately, with continuous stirring. The dispersion of the nanohybrid in the HBPEA matrix was aided using probe sonicator for a time period of 30 min. The nanocomposites obtained were then cured using bisphenol-A based epoxy resin (60:40 weight ratio of resin is to epoxy) and poly(amido amine) hardener (50 wt.% with respect to epoxy resin) [15]. The nanocomposites of HBPEA/nanohybrid with varying weight percentages of 1, 2.5 and 5 wt.% were coded as HBPEAC1, HBPEAC2.5 and HBPEAC5, respectively.

2.3. Antimicrobial activity

2.3.1. Antibacterial activity

The antibacterial assay of the prepared nanocomposites was performed using well diffusion method as described by Radhika et al. [19]. 200 μL of the log phase culture of the test microbes (10^{-7}–10^{-8} cell as per McFarland standard [20]) namely *Pseudomonas aeruginosa* (MTCC 7814), *Bacillus subtilis* (ATCC 11774), *Escherichia coli* (MTCC 40) and *Staphylococcus aureus* (ATCC 11632) was seeded on the surface of the Mueller Hinton agar medium. The prepared nanocomposites of varied weight percentages were dissolved in DMSO (10% v/v), filter-sterilized through a 0.22-μm membrane filter and then introduced into one of the wells (6 mm) in the agar plate. The samples were prepared in 10% DMSO (v/v) maintaining the concentrations of 0.1 g/mL. The test was performed using streptomycin sulfate (1 mg/mL) as a positive control and 10% DMSO as the negative control. The culture plates were incubated at (37 ± 2) °C for overnight and the observed zones of inhibition were measured using a transparent metric ruler. The reported results were averaged over a set of three independent experiments and the mean of inhibition diameters was determined.

2.3.2. Antifungal activity

The antifungal assay of the prepared samples was tested against different fungal strains viz., *Aspergillus niger*, *Fusarium oxysporum* (MTCC 284) and *Coleotricum capcii*. 200 μL of overnight grown culture (0.5–2.5 × 10^6 spores/mL as per McFarland standard) of the test fungal

strains was seeded on the surface of Sabouraud dextrose agar (SDA) medium. The experiments were performed in triplicate using Nystatin (1 mg/mL) as the positive control while 10% DMSO as the negative control. The growth inhibition was determined by measuring the diameter of inhibition zone post-overnight incubation at (25 ± 2) °C for 48 h.

2.3.3. Antialgal activity

Antialgal assay of the prepared samples was investigated against an algal consortium comprising of *Chlorella* sp., *Hormidium* sp. and *Cladophorella* sp. using modified solid Knop's medium [21]. An aliquot of 200 μL of fresh algal suspension was spread over the solidified Knop's medium using a sterilized glass spreader. The prepared film samples (2×1 cm^2) were then laid on the above solidified culture medium and then incubated at (25 ± 2) °C for a photoperiod of 15 h maintaining the humidity level of (83 ± 2)% for 5 weeks.

2.4. Characterization

The FTIR spectra of the pristine and nanocomposite samples were recorded by FTIR spectroscopy (Impact-410, Nicolet, USA) using KBr pellet. The dispersion of the nanohybrid in the HBPEA matrix was done using a standard sonotrode (tip-diameter 3 mm) in a high intensity ultrasonic processor (UP200S, Hielscher, Germany) at 60% amplitude and 0.5 cycles [22]. The technical specifications of the sonicator used for the preparation of the nanocomposite are as follows:

Usable/nominal output power: 200 W, Working frequency: 24 kHz, Control range: ±1 kHz, Output control: 20%–100%, steplessly adjusted, Pulse–pulse mode factor: 10%–100% per second, steplessly adjusted, Maximum energy density: 12–600 W/cm^2, depending on the sonotrode and, Maximum amplitude: 12–260 μm, depending on the sonotrode.

The thermogravimetric analysis was carried out in Shimadzu TGA 50 thermal analyzer at a nitrogen flow rate of 30 mL/min and at the heating rate of 10 °C/min. The tensile strength and elongation at break (as per the ASTM D 412-51T) of the cured thermosets were measured with the help of a Universal Testing Machine of model Zwick Z010 (Germany) by a 10 kN load cell and at 40 mm/min jaw separation speed. The gloss, scratch hardness and impact resistance of the cured films were measured as per the standard methods [23]. The scratch hardness test (ASTM D5178/1991) of the cured films was performed by a scratch hardness tester (Sheen instrument Ltd., UK). The front impact resistance test was carried out by applying falling ball method using an impact tester (S.C. Dey Co., Kolkata) with a maximum test height of 100 cm. In this test a weight of 850 g is allowed to fall on the film coated on a mild steel plate from minimum to maximum falling heights. The maximum height was taken as the impact resistance up to which the film was not damaged. The gloss characteristics of the cured films were measured using a mini glossmeter (Sheen instrument Ltd.,

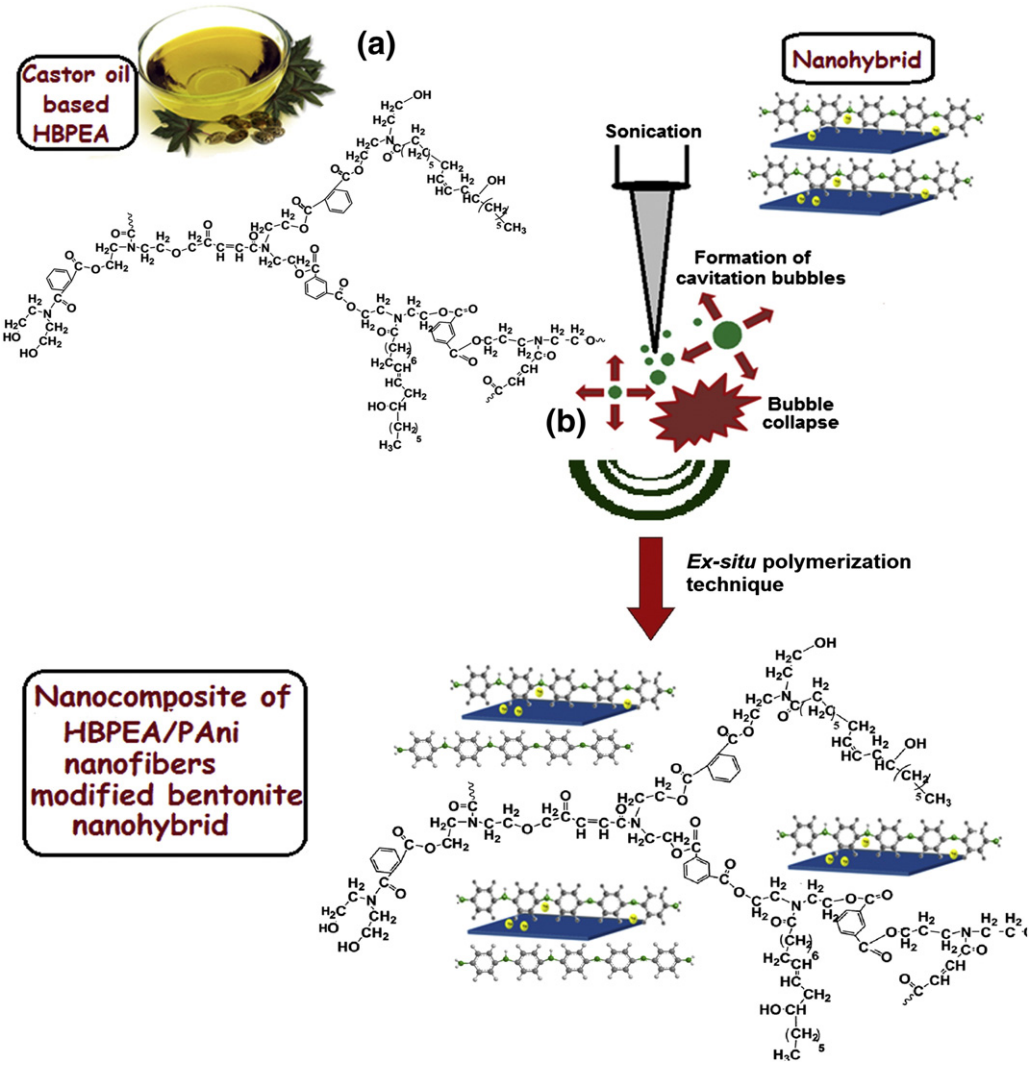

Fig. 1. Schematic representation of (a) the formation of the nanocomposites and (b) plausible mechanism of action.

UK) at an angle of incidence of 60°. The surface morphology of the thermoset was studied by a using JEOL 2100X electron microscope at operating voltage of 200 kV after casting on carbon coated copper grids.

3. Results and discussion

3.1. Ex-situ preparation of nanocomposites of HBPEA/nanohybrid

The ion exchange of the Na^+ cations from the MMT gallery by organo-polyaniline nanofibrous chains rendered structural modulation of the nanoclay surface for intercalation of HBPEA precursors. The cations present within the MMT interlayers were replaced with anilinium salts, which were then polymerized upon reaction with the ammonium peroxy sulfate oxidant. In other words, the PAni nanofiber intercalated via ionic bonds in the inorganic lamellae of the MMT [24]. The interaction between the PAni nanofiber and the MMT dictated the strength of the swollen tactoids and the modified interlayer spacing of the nanoplatelets available for diffusion of HBPEA chains.

3.2. Plausible mechanism of nanocomposite formation

Fig. 1 summarizes the mechanism of formation of the partially exfoliated structure of the nanocomposites. The PAni nanofiber intercalated/tethered onto MMT nanoplatelets provided a hydrophobic locale for HBPEA to diffuse into the nanoclay layers. Firstly, the swelling of the nanohybrid was controlled by the sorptive interactions between the THF dispersed organo-cations of the nanohybrid and the HBPEA, which dictated the initial accessibility of the nanosilicate galleries by the polymer chains. The polymer chains diffused and adhered onto the nanoplatelets at multiple sites of the nanosilicates, post-swelling action and resulted in a confined nanohybrid structure. Upon solvation of the nanohybrid, the inter-gallery polyanilinium cations reoriented from their initial monolayer, lateral bilayer and inclined paraffin structure to a perpendicular orientation with HBPEA chains inserted in between the organo-cations [25]. The ability of the PAni chains to reorient to a vertical position in order to optimize solvation interactions with HBPEA was the prerequisite for the loading the nanosilicate galleries with sufficient HBPEA content to obtain a layer exfoliation upon nanocomposite formation [25]. This charging of the nanohybrid galleries with the HBPEA primarily depended on the MMT charge density and the chain length of the organic modifier [25]. High layer charge density MMT required a large number of organo-cations to balance the charge difference of the nanoclay layers, which in turn paved way for lesser number of HBPEA chains to intercalate due to the presence of increased density of modifier organo-chains within the layers. In this context, MMT with a low layer charge density exhibited excellent swelling property and thus is proved to be the appropriate candidate for the formation of exfoliated nanocomposite system. A low density domain of PAni chains [13] within the MMT gallery provided more intergallery space to accommodate HBPEA chains, resulting in stronger elastic force within the nanohybrid galleries which effectively exerted strain on the nanoplatelets and compelled them to open up [26]. The hyperbranched structure of the resin was also instrumental in the increment of elastic forces within the nanohybrid. This low molecular weight HBPEA resin (2263 g/mol) has higher diffusibility as compared to its linear analog, which in turn helped to drive the HBPEA chains in between the nanohybrid platelets. Park and Jana reported that the exfoliation process starts at the nanosilicate layers and continues towards the center of the tactoid until the nanoplatelets are separated out [27]. The stacks of these nanoplatelets detach from the edge of the silicate layers, thereby initiating the formation of the exfoliated structure [28]. The continuous mechanical stirring aided in the dispersion of the nanohybrid layers in the polymer matrix. The nanohybrid galleries continued to expand with sonication resulting in the formation of the partial exfoliated nanocomposite architecture [29]. In other words, the formation and sudden collapse of small cavitation bubbles as a function of rarefaction and compression cycles of sonication resulted in the formation of microjets (release of large amount of energy) [22] which helped in partial exfoliation of the nanohybrid platelets, as evident from the HRTEM study. The interfacial interactions between silicate layers of the nanohybrid and the polar moieties of the HBPEA matrix helped to enlarge the layer spacing and break the basal plane stacking of the nanoplatelets to induce exfoliated structure, which is further confirmed from the XRD study.

3.3. FTIR analysis

The FTIR spectra of HBPEA, nanohybrid, HBPEAC1, HBPEAC2.5 and HBPEAC5 are shown in Fig. 2(a–e). The FTIR bands of the nanohybrid appeared at 529, 1437 and 1483 cm^{-1} which are ascribed to the Si–O–Al, Si–O–Si and C=C benzenoid ring stretching, respectively [13]. The characteristic bands of HBPEA corresponding to –C=O appeared at 1730 cm^{-1}, amide group at 1632 cm^{-1} and hydrogen bonded –OH stretching at 3420 cm^{-1} (Fig. 2a) [15]. The bands of nanohybrid were found to be retained upon the formation of the nanocomposite system, although with slight shifting in the wavenumber values. The stretching frequency of carbonyl ester and amide shifted to 1725 and 1637 cm^{-1} upon the formation of the nanocomposite system. This shifting of the FTIR bands in the nanocomposites as compared to the pristine polymer was attributed to the interaction of the nanohybrid with the HBPEA chains. The red shifting of the carbonyl ester band in the nanocomposites was attributed to the interaction of the same with the nitrogenous groups of PAni chains in the nanohybrid. The blue shifting of the carbonyl amide band was ascribed to the hydrogen bonding with the –NH– group of the nanohybrid. The H-bonding was further confirmed from the broadening of the –OH band in the FTIR bands of the nanocomposites as compared to the pristine polymer.

3.4. HRTEM study

The distribution of the partially exfoliated nanoplatelets of the nanohybrid in the HBPEA matrix was evidenced from the HRTEM micrographs (Fig. 3). The images of the nanocomposites (Fig. 3a–c)

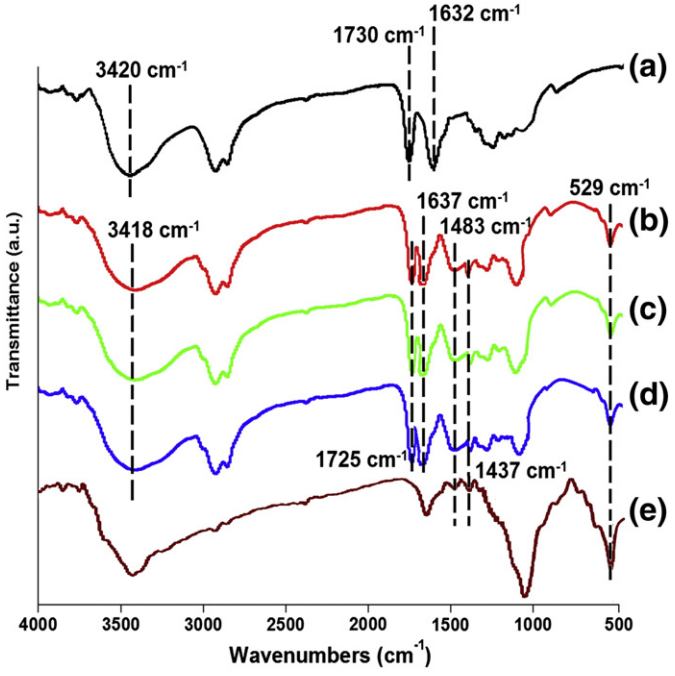

Fig. 2. FTIR spectra of (a) HBPEA, (b) HBPEAC1, (c) HBPEAC2.5, (d) HBPEAC5 and (e) nanohybrid.

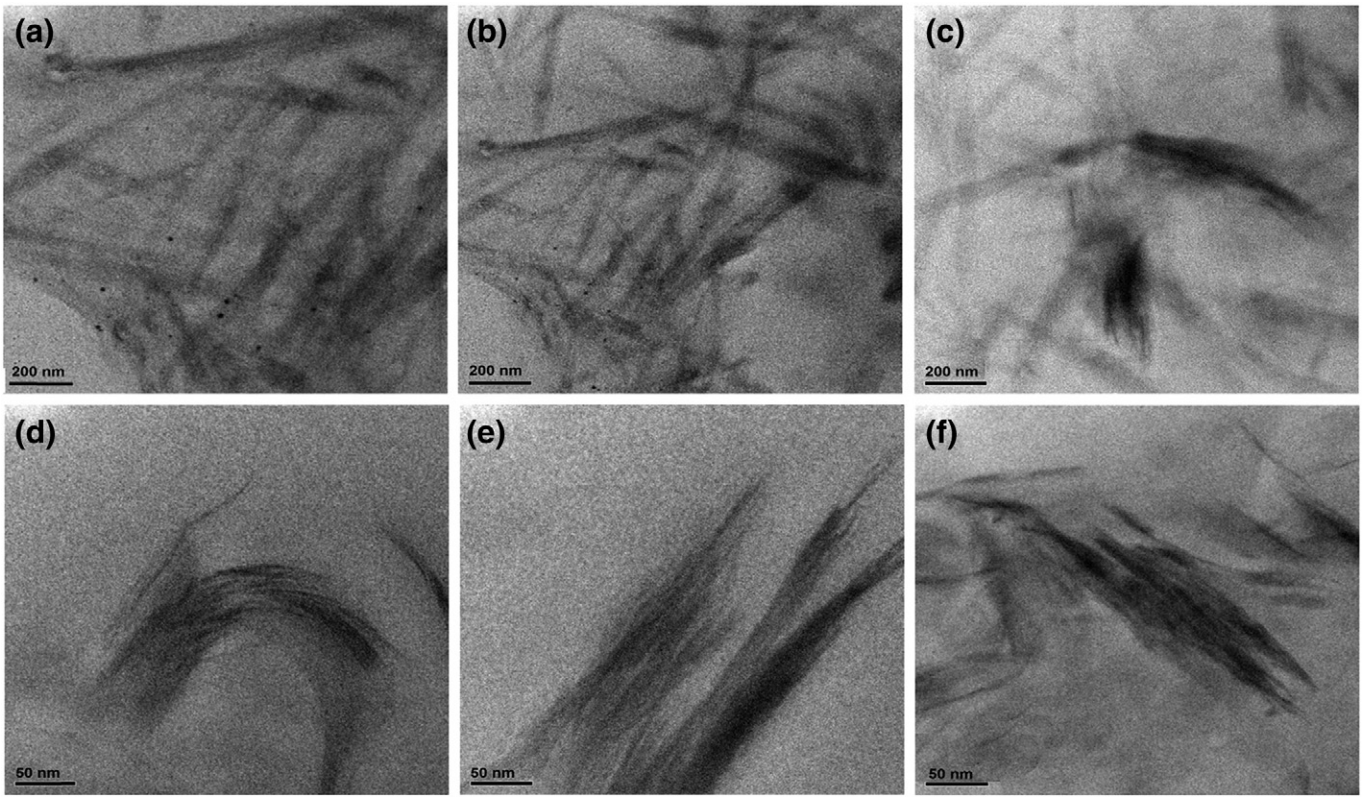

Fig. 3. HRTEM micrographs of HBPEAC1 (a) and (d), HBPEAC2.5 (b) and (e), HBPEAC5 (c) and (f), at magnification scale bar of 200 nm and 50 nm, respectively.

with a scale bar of 200 nm exhibited a uniform distribution of the nanoplatelets within the HBPEA matrix. The HRTEM micrographs at higher magnification scale bar of 50 nm (Fig. 3d–f) revealed the formation of partially exfoliated structure of the nanocomposite systems, although a few stacks of the nanohybrid were observed along with the exfoliated layers at higher loading of 5 wt.%. It is inferred, thus, from Fig. 3(b) that the partial exfoliation of the nanocomposites has taken placed by the delamination of the nanoplatelets. This exfoliation did not occur by the removal of the platelets (sheet by sheet), as an independent process of intercalation [30]. Instead, the exfoliation process started from the edge of the nanolayers and fanning away in outward direction.

3.5. XRD study

The XRD patterns of HBPEA, nanohybrid, HBPEAC1, HBPEAC2.5 and HBPEAC5 thermosets are shown in Fig. 4(a–e). The characteristic diffraction peaks of nanohybrid appeared at around $2\theta = 5.8°$, 19.2° and 26°, attributed due to the (001), (100) and (110) planes of MMT and HCl doped PAni in parallel orientation and perpendicular orientation, respectively [13]. The pristine HBPEA exhibited a broad XRD peak, which was attributed to its amorphous structure. The (001) basal diffraction peak of the nanohybrid disappeared upon the formation of the nanocomposite system. However, the diffraction peak at around 19–20° reflected the interaction of HBPEA with the (100) plane of the PAni chains of the nanohybrid.

The absence of (001) basal plane gave an inkling about the partial exfoliation of the nanohybrid tactoids with no regular repeating distance between the individual nanoplatelets of the nanocomposite system [31]. This was further supported by the reports of Lan et al. [25] that the modification of MMT using primary and secondary onium ions formed exfoliated nanocomposites, whereas those using tertiary and quaternary onium ions retained the tactoid structure, prototype of the intercalated ones. Thus MMT modified using secondary anilinium ions of the PAni exhibited partially exfoliated structure upon the formation of the nanocomposite with the HBPEA matrix.

3.6. Performance study

The performance of the epoxy-poly(amido amine) cured thermosetting nanocomposites effectively changed with the incorporation of varying amounts of the nanohybrid (Table 1). It was found that the curing time of the epoxy-poly(amido amine) cured HBPEA and its nanocomposites baked at 150 °C, decreased drastically with the increase of

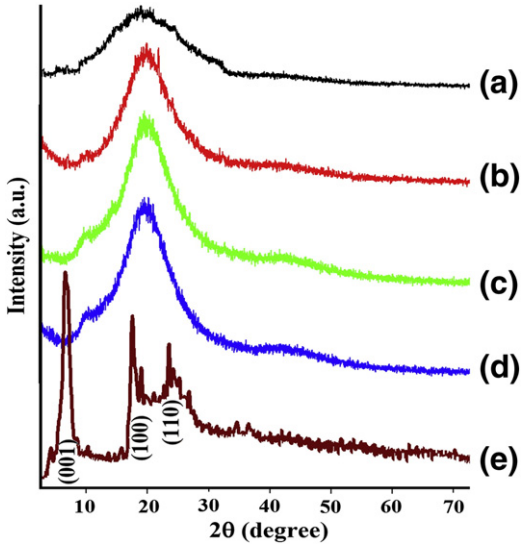

Fig. 4. XRD diffractograms of (a) HBPEA, (b) HBPEAC1, (c) HBPEAC2.5, (d) HBPEAC5 and (e) nanohybrid.

Table 1
Performance of HBPEA, HBPEAC1, HBPEAC2.5 and HBPEAC5 thermosets.

Physico-mechanical property	HBPEA	HBPEAC1	HBPEAC2.5	HBPEAC5
Curing time (h)	10	2.5	2.2	2.0
Gel fraction (%)	77	78	79.2	80
Scratch hardness (kg)	8.5	9	9.5	10
Impact resistance (cm)	100	100	100	100
Gloss at 60°	90	91	92.5	95
Tensile strength (MPa)	7.2	8.9	11.4	14.3
Elongation at break (%)	88.2	85.1	84.5	82.6

the nanohybrid content. This was attributed to the PAni chains which catalyzed the intra-gallery curing reaction between HBPEA, epoxy and poly(amido amine). The curing reaction and the possible interactions of the HBPEA and nanohybrid with the epoxy and poly(amido amine) hardener are shown in Fig. 5. The increment in the gloss with the increase in the nanohybrid content in the nanocomposites indicated that the cured thermosets possessed good dimensional stability and smooth surface texture. This was attributed to the basic nature of the amine groups present in the partially exfoliated nanohybrid which aided in the crosslinking reaction of the resin. The increment of scratch hardness of the nanocomposites with nanohybrid content was due to the enhanced strength and flexibility of the HBPEA chains. The high impact resistance of the thermosets showed optimum crosslinking and flexibility of the long hydrocarbon chains of HBPEA.

The nanoscale dispersion and interfacial interaction of the partially exfoliated nanohybrid and HBPEA optimized the mechanical properties of the nanocomposites [32]. The pristine HBPEA thermoset has a tensile strength of 7.2 MPa which increased from 8.9 to 14.3 MPa with the increment in the nanohybrid content from 1 to 5 wt.%. The two-fold improvement in the mechanical properties of the 5 wt.% nanohybrid containing nanocomposite was attributed to the interfacial interaction between the resin and the nanohybrid, as evident from the FTIR study. Moreover the high aspect ratio PAni nanofiber absorbed onto the exfoliated nanohybrid layers [13] affords reinforcing action to the nanocomposites. The decrease of elongation at break (EB) of the thermosetting nanocomposites (Table 1) with the increase in the nanohybrid content was ascribed to the restricted mobility of the HBPEA chains at the nanoplatelet interface due to interaction of the HBPEA with the high surface area of the nanoplatelets (Table 1). However the decrease in the EB was not much pronounced because of the plasticization effect of the long polymeric organo-modifier chains of PAni nanofiber.

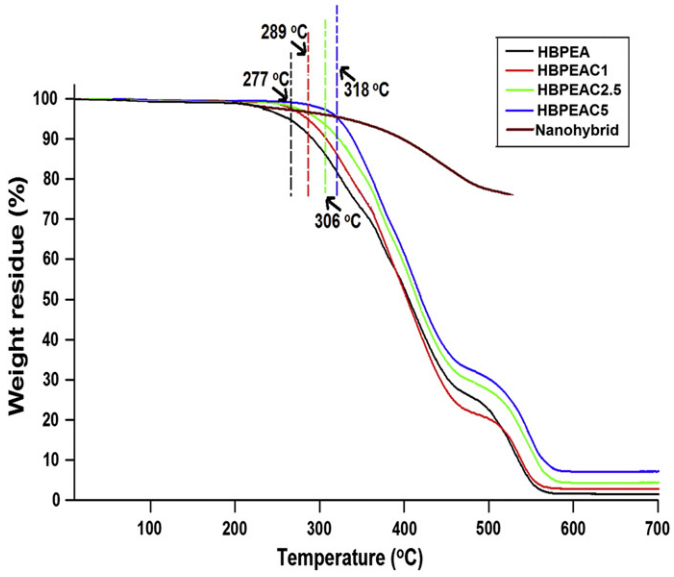

Fig. 6. TGA thermograms of HBPEA, HBPEAC1, HBPEAC2.5, HBPEAC5 and nanohybrid.

3.7. Thermal study

The HBPEA and thermosetting nanocomposites exhibited a two-step degradation pattern (Fig. 6) with dose-dependent increase of thermal stability. The nanohybrid possessed high thermal stability above 450 °C with only 6–8 wt.% loss due to water molecules present within the nanoclay layers through hydrogen bonding [13]. The HBPEA exhibited thermal stability up to 277 °C, while the onset thermal degradation increased to 318 °C upon incorporation of 5 wt.% nanohybrid into the polymer matrix. The increment in the thermal stability of the nanocomposites as compared to that of the pristine HBPEA was attributed to the dense and stable dispersion of the partially exfoliated nanosilicate layers, which aided in the increase of the intra-gallery crosslinking

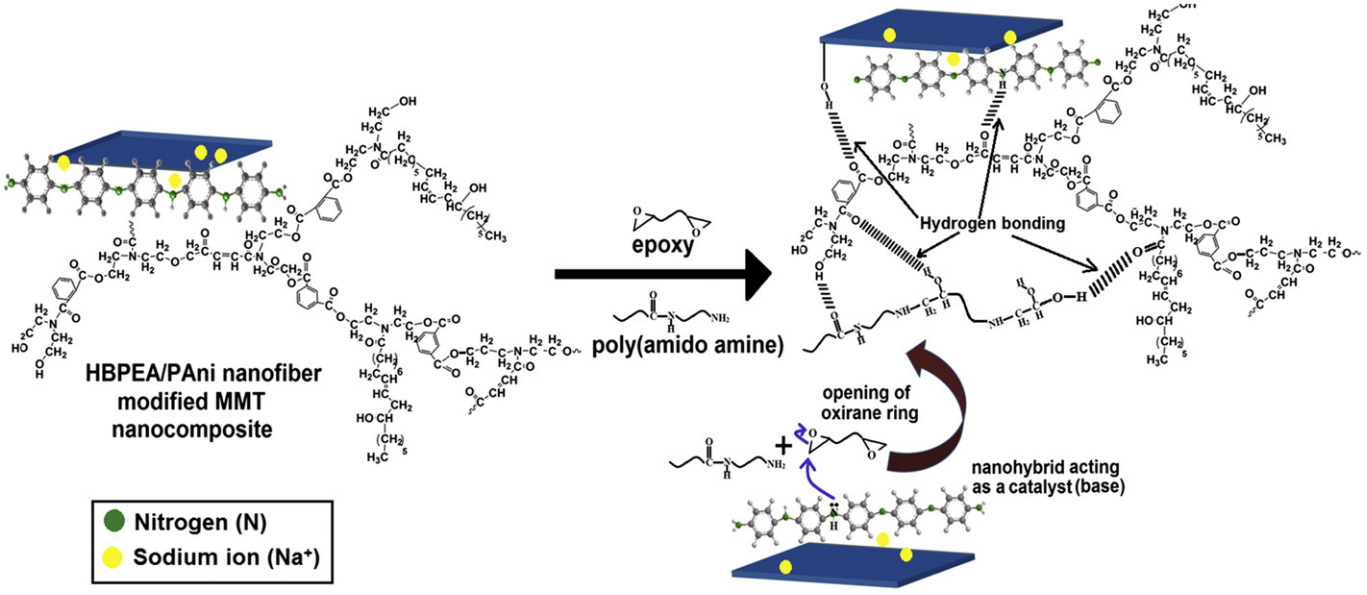

Fig. 5. Possible interactions and curing reaction of the HBPEA and nanohybrid using epoxy-poly(amido amine) hardener system.

Table 2
Antimicrobial potency of HBPEA, HBPEAC1, HBPEAC2.5 and HBPEAC5.

Test organism	Zone of inhibition (mm)				
	Control	HBPEA	HBPEAC1	HBPEAC2.5	HBPEAC5
P. aeruginosa[a]	18	9	11	12	13
E. coli[a]	24	9	10	11	12
B. subtilis[a]	18	10	12	14	15
S. aureus[a]	18	11	12	13	15
A. niger[b]	16	10	12	12	15
F. oxysporum[b]	14	9	10	11	12
C. capcii[b]	16	9	12	14	15
Algal consortium[c]	√	×	√	√	√

[a] Streptomycin sulfate was taken as positive control for bacterial strains.
[b] Nystatin sulfate was taken as positive control for fungal strains.
[c] √: positive antialgal activity, ×: negative antialgal activity.

reaction. The increment in the thermal stability of the nanocomposites with the increase of nanohybrid content was attributed to the nanoplatelets of the nanohybrid which act as a heat barrier and enhanced the overall thermal stability of the nanocomposites together with assisting in the formation of char upon thermal decomposition. The PAni nanofiber present in the nanohybrid also played an important role in the enhancement of the thermal stability of the nanocomposites by acting as a bridge between the nanoplatelets and HBPEA chains.

3.8. Antimicrobial activity

The mean zones of inhibition observed in the antibacterial and antifungal tests are tabulated in Table 2.

Fig. 7 depicts representative culture plates showing antibacterial activity of HBPEA, HBPEAC1, HBPEAC2.5 and HBPEAC5. The HBPEA exhibited comparatively less antibacterial activity against the tested bacterial strains than the nanocomposites. The zone of inhibition of the antibacterial tests of the nanocomposites increased with the increase in the incorporation of the nanohybrid content in the HBPEA matrix, with the zones of inhibition in a range of 10–15 mm. The nanocomposites exhibited pronounced antibacterial efficacy against *B. subtilis* and *S. aureus* as compared to the *P. aeruginosa* and *E. coli*. It was thus inferred from the above observations that the nanocomposites were more effective against Gram positive bacteria as compared to the Gram negative ones, showing differential interaction of the same with the molecular moieties present on the surface of the two different bacterial groups. The basic architectural differences between the cell wall structures in the two bacterial groups may play a key role in the determination of their antibacterial activities [33]. The inhibition of the bacterial growth by the nanocomposites was attributed to the presence of the emeraldine salt form of PAni nanofiber of the nanohybrid in the partially exfoliated nanocomposites. The pronounced antibacterial activity of the emeraldine salt form of PAni was attributed due to its structural similarity with that of the active antibacterial compound tetracyclines, which inhibit the protein synthesis in the bacterial cells through bacteriostatic mode of action [34].

The representative culture plates showing antifungal activity of HBPEA, HBPEAC1, HBPEAC2.5 and HBPEAC5 are shown in Fig. 8. The results showed that the materials exhibited potent biocidal activity against *A. niger*, *F. oxysporum*, and *C. capcii*. The well diffusion method of the tested samples showed clear inhibition zone of 10–14 mm (Table 2). The antifungal activity of the HBPEA may be attributed to the binding affinity of the same with the ergosterol, an essential component of the cell membrane for the normal growth and viability of fungal

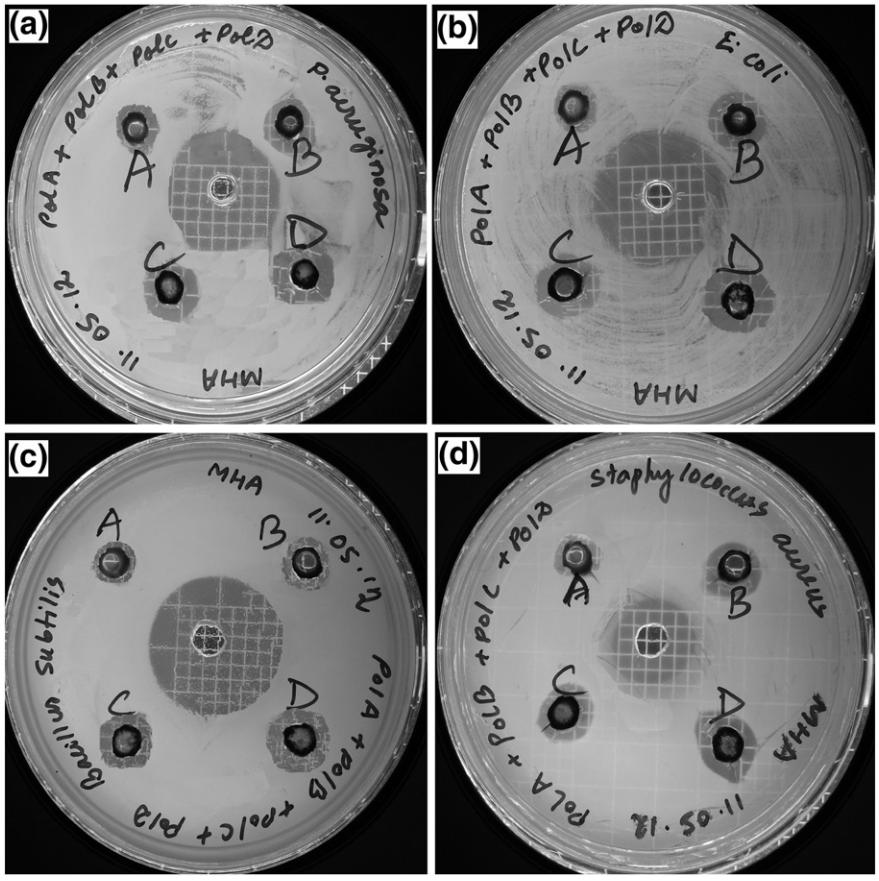

Fig. 7. Representative culture plates showing antibacterial activity of HBPEA, HBPEAC1, HBPEAC2.5 and HBPEAC5 against (a) *Pseudomonas aeruginosa*, (b) *Escherichia coli*, (c) *Bacillus subtilis* and (d) *Staphylococcus aureus*.

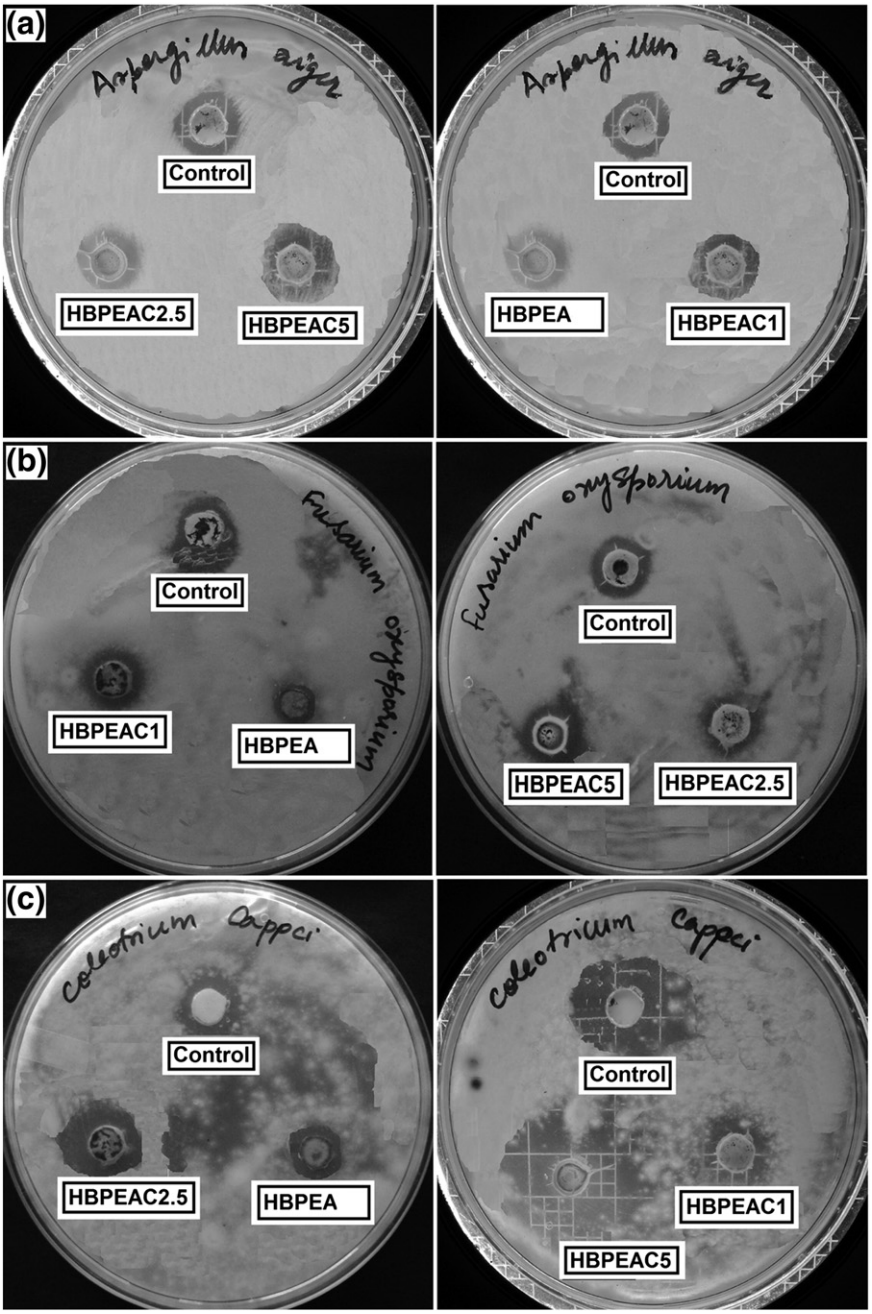

Fig. 8. Representative culture plates showing antifungal activity of HBPEA, HBPEAC1, HBPEAC2.5 and HBPEAC5 against (a) *Aspergillus niger*, (b) *Fusarium oxysporum* and (c) *Coleotricum capcii*.

cells [35]. The hyperbranched architecture of the nanocomposites bequeathed with multiple functionalities and large free volume space provided greater accessibility and interaction of the polymer chains with the microbial cells. The interaction of the long fatty acid chains of pristine polymer and nanocomposites with the cellular ergosterol composition of the fungi may be a probable cause of the inhibitory action. The improved antifungal activity of the nanocomposites may also be attributed to the presence of benzyl amine structure in the PAni backbone of the nanohybrid, which interferes with the production of ergosterol [36].

The antialgal assay examined the ability of the pristine and nanocomposite samples to inhibit the growth of an algal consortium constituting of *Chlorella*, *Hormidium* and *Cladophorella* species. The results of antialgal assay of HBPEA, HBPEAC1, HBPEAC2.5 and HBPEAC5 are summarized in Table 2. The light source used for the above test emitted trace amounts of ultraviolet (UV) light particularly UVA (400–315 nm) and UVC (280–100 nm). The probable mode of antialgal activity of the nanocomposites was attributed due to the UVA absorption by the PAni nanofiber (at around 340 nm) [37] of the exfoliated nanohybrid platelets and funneling it to the algal cells, which in turn hampered their photosynthesis process, thereby posing a risk to their growth and replication.

However, the establishment of the molecular level interaction mechanism for the antimicrobial activity of the nanocomposites needs further delving employing multi-disciplinary integrated approach.

4. Conclusions

The present study highlighted the mechanism of formation of partial exfoliated nanocomposites of bio-based HBPEA and PAni nanofiber modified MMT. The low charge density nanohybrid provided the nanocomposites with partial layer exfoliated structure. The FTIR

study vouched for the interaction of the nanohybrid with the HBPEA matrix. HRTEM envisaged the formation of partially exfoliated structure of the prepared nanocomposites. The onset degradation temperature of the nanocomposites shifted to higher temperature as compared to the pristine HBPEA thermoset. The antimicrobial activity of the nanocomposites against broad spectrum microbes including bacteria and fungi as well as algal consortium, increased with the nanohybrid content. The nanocomposites possessed potent antimicrobial properties with added facet of desirable physico-mechanical properties and thermal stability to find applications as bio-based multi-functional antimicrobial materials in the biomedical devices.

Acknowledgments

The authors express their gratitude and thanks to the research project assistance given by DRL, India, through grant No. DRL/1047/TC, dated 2nd March, 2011, SAP (UGC), India through grant No. F.3-30/2009(SAP-II) and FIST program-2009 (DST), India through grant No. SR/FST/CSI-203/209/1 dated 06.05.2010. Sophisticated Analytical Instrument Facility (SAIF), North Eastern Hill University (NEHU) Shillong is thankfully acknowledged for the TEM imaging.

References

[1] V. Bugatti, G. Gorrasi, F. Montanari, M. Nocchetti, L. Tammaro, V. Vitttoria, Modified layered double hydroxides in polycaprolactone as a tunable delivery system: in vitro release of antimicrobial benzoate derivatives, Appl. Clay Sci. 52 (2011) 34–40.
[2] V. Sambhy, M.M. MacBride, B.R. Peterson, A. Sen, Silver bromide nanoparticle/polymer composites: dual action tunable antimicrobial materials, J. Am. Chem. Soc. 128 (2006) 9798–9808.
[3] K. Galiano, C. Pleifer, K. Engelhardt, G. Brössner, P. Lackner, C. Huck, C. Lass-Flörl, A. Obwegeser, Silver segregation and bacterial growth of intraventricular catheters impregnated with silver nanoparticles in cerebrospinal fluid drainages, Neurol. Res. 30 (2008) 285–287.
[4] A.J. Huh, Y.J. Kwon, "Nanoantibiotics": a new paradigm for treating infectious diseases using nanomaterials in the antibiotics resistant era, J. Control. Release 156 (2011) 128–145.
[5] Q. Jia, S. Shan, L. Jiang, Y. Wang, D. Li, Synergistic antimicrobial effects of polyaniline combined with silver nanoparticles, J. Appl. Polym. Sci. 125 (2012) 3560–3566.
[6] Z. Du, C. Li, L. Li, M. Zhang, S. Xu, T. Wang, Simple fabrication of a sensitive hydrogen peroxide biosensor using enzymes immobilized in processable polyaniline nanofibers/chitosan film, Mater. Sci. Eng. C 29 (2009) 1794–1797.
[7] S. Pramanik, R. Konwarh, R.C. Deka, L. Aidew, N. Barua, A.K. Buragohain, D. Mohanta, N. Karak, Microwave-assisted poly(glycidyl methacrylate)functionalized multiwall carbon nanotubes with a 'tendrillar' nanofibrous polyaniline wrapping and their interaction at bio-interface, Carbon 55 (2013) 34–43.
[8] B. Girase, D. Depan, J.S. Shah, W. Xu, R.D.K. Misra, Silver–clay nanohybrid structure for effective and diffusion-controlled antimicrobial activity, Mater. Sci. Eng. C 31 (2011) 1759–1766.
[9] M. Mravcakova, K. Boukerma, M. Omastova, M.M. Chehimi, Montmorillonite/polypyrrole nanocomposites. The effect of organic modification of clay on the chemical and electrical properties, Mater. Sci. Eng. C 26 (2006) 306–313.
[10] G. Chandrasekaran, H.K. Han, G.J. Kim, H.J. Shin, Antimicrobial activity of delaminated aminopropyl functionalized magnesium phyllosilicates, Appl. Clay Sci. 53 (2011) 729–736.
[11] B.H. Kim, J.H. Jung, S.H. Hong, J. Joo, Nanocomposites of polyaniline and Na+-montmorillonite clay, Macromolecules 35 (2002) 1419–1423.
[12] R. Alizadeh, J.J. Beaudoin, L. Raki, V. Terskikh, C-S-H/polyaniline nanocomposites prepared by in situ polymerization, J. Mater. Sci. 46 (2011) 460–467.
[13] S. Pramanik, G. Das, N. Karak, Facile preparation of polyaniline nanofibers modified bentonite nanohybrid for gas sensor application, RSC Adv. 3 (2013) 4574–4581.
[14] S.C.M. Fernandes, P. Sadocco, A.A. Varona, T. Palomares, A. Eceiza, A.J.D. Silvestre, I. Mondragon, C.S.R. Freire, Bioinspired antimicrobial and biocompatible bacterial cellulose membranes obtained by surface functionalization with aminoalkyl groups, ACS Appl. Mater. Interfaces 5 (2013) 3290–3297.
[15] S. Pramanik, R. Konwarh, K. Sagar, B.K. Konwar, N. Karak, Bio-degradable vegetable oil based hyperbranched poly(ester amide) as an advanced surface coating material, Prog. Org. Coat. 76 (2013) 689–697.
[16] R.S. Rajeev, E. Harkin-Jones, K. Soon, T. McNally, G. Menary, C.G. Armstrong, P.J. Martin, Studies on the effect of equi-biaxial stretching on the exfoliation of nanoclays in polyethylene terephthalate, Eur. Polym. J. 45 (2009) 332–340.
[17] A.M. Bonilla, M.F. Garcia, Polymeric materials with antimicrobial activity, Prog. Polym. Sci. 37 (2012) 281–339.
[18] S. Pramanik, K. Sagar, B.K. Konwar, N. Karak, Synthesis, characterization and properties of a castor oil modified biodegradable poly(ester amide) resin, Prog. Org. Coat. 75 (2012) 569–578.
[19] P. Radhika, B.S. Sastry, B.M. Harica, Antimicrobial screening of *Andrographis paniculata* (Acanthaceae) root extracts, Res. J. Biotech. 3 (2008) 62–63.
[20] J.M. Andrews, BSAC standardized disc susceptibility testing method (version 4), J. Antimicrob. Chemother. 56 (2005) 60–76.
[21] C.C. Gaylarde, P.M. Gaylarde, A comparative study of the major microbial biomass of biofilms on exteriors of buildings in Europe and Latin America, Int. Biodeterior. Biodegrad. 55 (2005) 131–139.
[22] R. Konwarh, S. Pramanik, D. Kalita, C.L. Mahanta, N. Karak, Ultrasonication—a complementary 'green chemistry' tool to biocatalysis: a laboratory-scale study of lycopene extraction, Ultrason. Sonochem. 19 (2012) 292–299.
[23] U. Konwar, N. Karak, Mesua ferrea L. seed oil-based highly branched polyester resins, Polym. Plast. Technol. Eng. 48 (2009) 970–975.
[24] V. Bugatti, L. Esposito, L. Franzetti, L. Tammaro, V. Vittoria, Influence of the powder dimensions on the antimicrobial properties of modified layered double hydroxide, Appl. Clay Sci. 75–76 (2013) 46–51.
[25] T. Lan, P.D. Kaviratna, T.J. Pinnavaia, Mechanism of clay tactoid–tactoid exfoliation in epoxy-clay nanocomposites, Chem. Mater. 7 (1995) 2144–2150.
[26] M.J. Gintert, S.C. Jana, S.G. Miller, Evaluation of nanoclay exfoliation strategies for thermoset polyimide nanocomposite systems, Proceedings of Antec. BritainNASA Glenn Research Center, Cleveland, 2007, pp. 1399–1403.
[27] J. Park, S. Jana, Mechanism of exfoliation of nanoclay particles in epoxy-clay nanocomposites, Macromolecules 36 (2003) 2758–2768.
[28] Z. Martin, I. Jimenez, M.A. Gomez, H.W. Ade, D.A. Kilcoyne, D.H. Cruz, Spectromicroscopy study of intercalation and exfoliation in polypropylene/montmorillonite nanocomposites, J. Phys. Chem. B 113 (2009) 11160–11165.
[29] M. Haq, R. Burgueño, A.K. Mohanty, M. Misra, Processing techniques for bio-based unsaturated-polyester/clay nanocomposites: tensile properties, efficiency, and limits, Compos. Part A 40 (2009) 394–403.
[30] W. Xu, L. Guodong, W. Wang, S. Tang, P. He, W.P. Pan, PP–PP-g-MAH–org-MMT nanocomposites. I. intercalation behavior and microstructure, J. Appl. Polym. Sci. 88 (2002) 3225–3231.
[31] A. Kaushik, D. Ahuja, V. Salwani, Synthesis and characterization of organically modified clay/castor oil based chain extended polyurethane nanocomposites, Compos. Part A 42 (2011) 1534–1541.
[32] R. Ollier, E. Rodriguez, V. Alvarez, Unsaturated polyester/bentonite nanocomposites: influence of clay modification on final performance, Compos. Part A 48 (2013) 137–143.
[33] S. Pramanik, R. Konwarh, N. Barua, A.K. Buragohain, N. Karak, Bio-based hyperbranched poly(ester amide)/MWCNT nanocomposites: multimodalities at biointerface, Biomater. Sci. http://dx.doi.org/10.1039/C3BM60170F.
[34] C. Sun, D.K. Hunt, R.B. Clark, D. Lofland, W.J.O. Brien, L. Plamondon, X.Y. Xiao, Synthesis and antibacterial activity of pentacyclines: a novel class of tetracycline analogs, J. Med. Chem. 54 (2011) 3704–3731.
[35] W. Iwatani, T. Arika, H. Yamaguchi, Two mechanisms of butenafine action in *Candida albicans*, Antimicrob. Agents Chemother. 37 (1993) 785–788.
[36] T. Mironava, M. Hadjiargyrou, M. Simon, M.H. Rafailovich, The effects of UV emission from compact fluorescent light exposure on human dermal fibroblasts and keratinocytes in vitro, Photochem. Photobiol. 88 (2012) 1497–1506.
[37] S. Pramanik, N. Karak, S. Banerjee, A. Kumar, Effects of solvent interactions on the structure and properties of prepared PAni nanofibers, J. Appl. Polym. Sci. 126 (2012) 830–836.